

## Surface Chemistry on Bimetallic Alloy Surfaces: Adsorption of Anions and Oxidation of CO on Pt<sub>3</sub>Sn(111)

Vojislav R. Stamenković,<sup>†</sup> Matthias Arenz,<sup>†</sup> Christopher A. Lucas,<sup>‡</sup>  
Mark E. Gallagher,<sup>‡</sup> Philip N. Ross,<sup>†</sup> and Nenad M. Marković<sup>\*,†</sup>

Contribution from the Materials Sciences Division, Lawrence Berkeley National Laboratory,  
University of California, Berkeley, California 94720, and Oliver Lodge Laboratory,  
Department of Physics, University of Liverpool, Liverpool, L69 7ZE, UK

Received December 7, 2002; E-mail: nmmarkovic@lbl.gov

**Abstract:** The microscopic structure of the Pt<sub>3</sub>Sn(111) surface in an electrochemical environment has been studied by a combination of ex situ low-energy electron diffraction (LEED), Auger electron spectroscopy (AES), and low-energy ion scattering (LEIS) and in situ surface X-ray scattering (SXS) and Fourier transform infrared (FTIR) spectroscopy. In ultrahigh vacuum (UHV) the clean-annealed surface produces a  $p(2 \times 2)$  LEED pattern consistent with the surface composition, determined by LEIS, of 25 at. % Sn. SXS results show that the  $p(2 \times 2)$  structure can be "transferred" from UHV into 0.5 M H<sub>2</sub>SO<sub>4</sub> and that the surface structure remains stable from 0.05 to 0.8 V. At 0.05 V the expansion of Pt surface atoms, ca. +2% from the bulk lattice spacing, is induced by adsorption of underpotential-deposited (UPD) hydrogen. At 0.5 V, where Pt atoms are covered by (bi)sulfate anions, the topmost layer is contracted relative to 0.05 V, although Sn atoms expand significantly, ca. 8.5%. The  $p(2 \times 2)$  structure is stable even in solutions containing CO. In contrast to the Pt(111)–CO system, no ordered structures of CO are formed on the Pt<sub>3</sub>Sn(111) surface and the topmost layer expands relatively little (ca. 1.5%) from the bulk lattice spacing upon the adsorption of CO. The binding site geometry of CO on Pt<sub>3</sub>Sn(111) is determined by FTIR. In contrast to the near invariant band shape of a-top CO on Pt(111), changes in band morphology (splitting of the band) and vibrational properties (increase in the frequency mode) are clearly visible on the Pt<sub>3</sub>Sn(111) surface. To explain the line shape of the CO bands, we suggest that in addition to alloying effects other factors, such as intermolecular repulsion between coadsorbed CO and OH species, are controlling segregation of CO into cluster domains where the local CO coverage is different from the coverage expected for the CO–CO interaction on an unmodified Pt(111) surface.

### 1. Introduction

For over a decade now the ability to characterize atomic/molecular spatial structures and to monitor changes in the local symmetry of surface atoms in situ under the reaction conditions has played an important part in our understanding of surface electrochemistry at metal-based interfaces. This progress has been influenced greatly by the development of in situ surface sensitive probes<sup>1–8</sup> and vibrational spectroscopies,<sup>9–12</sup> which

in combination with classical electrochemical methods<sup>13–15</sup> have been used to find interrelationships between the microscopic surface structures of fcc metals (Pt, Ir, Pd, Au, Ag, Cu) and the macroscopic kinetic rates of the reactions. As for pure metals, considerable effort has also been directed to the study of surface electrochemistry on well-characterized Pt-bimetallic surfaces, which can be prepared either by deposition of one metal on the surface of another<sup>16,17</sup> or, using conventional metallurgy, as bulk alloys.<sup>18,19</sup> While for the former systems significant progress has been made,<sup>15</sup> for the bulk alloys there is still much to be understood regarding both adsorptive chemistry and electrocatalytic properties at the atomic levels.

Pt<sub>3</sub>Sn(111) is one of the most active systems known for CO oxidation. In this paper we attempt to provide insight into the

<sup>‡</sup> University of Liverpool.

<sup>†</sup> University of California.

- (1) Samant, M. G.; Toney, M. F.; Borges, G. L.; Blurton, K. F.; Melroy, O. R. *J. Phys. Chem.* **1988**, *92*, 220.
- (2) Ocko, B. M.; Wang, J.; Davenport, A.; Isaacs, H. *Phys. Rev. Lett.* **1990**, *65*, 1466–1469.
- (3) Toney, M. F.; Ocko, B. M. *Synchrotron Radiation News* **1993**, *6*, 28–33.
- (4) Tidswell, I. M.; Markovic, N. M.; Ross, P. N. *Phys. Rev. Lett.* **1993**, *71*, 1601–1604.
- (5) Lucas, C.; Markovic, N. M.; Ross, P. N. *Surf. Sci.* **1996**, *340*, L949–L954.
- (6) Lucas, C.; Markovic, N. M.; Ross, P. N. *Phys. Rev. Lett.* **1996**, *77*, 4922–4925.
- (7) Itaya, K. *Prog. Surf. Sci.* **1998**, *58*, 121–247.
- (8) Kolb, D. M. *Prog. Surf. Sci.* **1996**, *51*, 109–173.
- (9) Faguy, P. W.; Markovic, N.; Adzic, R. R.; Fierro, C. A.; Yeager, E. B. *J. Electroanal. Chem.* **1990**, *289*, 245–262.
- (10) Nichols R. J. Imaging Metal Electrocrystallization at High Resolution. *Frontiers of Electrochemistry*; Lipkowsky, J., Ross P. N., Eds.; Wiley-VCH: New York, 1999; pp 99–137.
- (11) Sawatari, Y.; Inukai, J.; Ito, M. *J. Electron Spec.* **1993**, *64/65*, 515–522.

- (12) Nart, F. C.; Iwasita, T.; Weber, M. *Electrochim. Acta* **1994**, *39*, 961.
- (13) Pleskov, Y. V.; Filinovskij, V. Y. *The Rotating Disc Electrode*; Consultant Bureau: New York, 1976.
- (14) Bard, A. J.; Faulkner, L. R. *Electrochemical Methods*; Wiley & Sons: New York, 1980; p 283.
- (15) Markovic, N. M.; Ross, P. N. *Surf. Sci. Rep.* **2002**, *45*, 121–254.
- (16) Watanabe, M.; Motoo, S. *J. Electroanal. Chem.* **1975**, *60*, 259–266.
- (17) Watanabe, M.; Motoo, S. *J. Electroanal. Chem.* **1975**, *60*, 275–283.
- (18) Gasteiger, H. A.; Markovic, N.; Ross, P. N.; Cairns, E. J. *J. Phys. Chem.* **1994**, *98*, 617–625.
- (19) Gasteiger, H. A.; Markovic, N. M.; Ross, P. N. *J. Phys. Chem.* **1995**, *99*, 8945–8949.

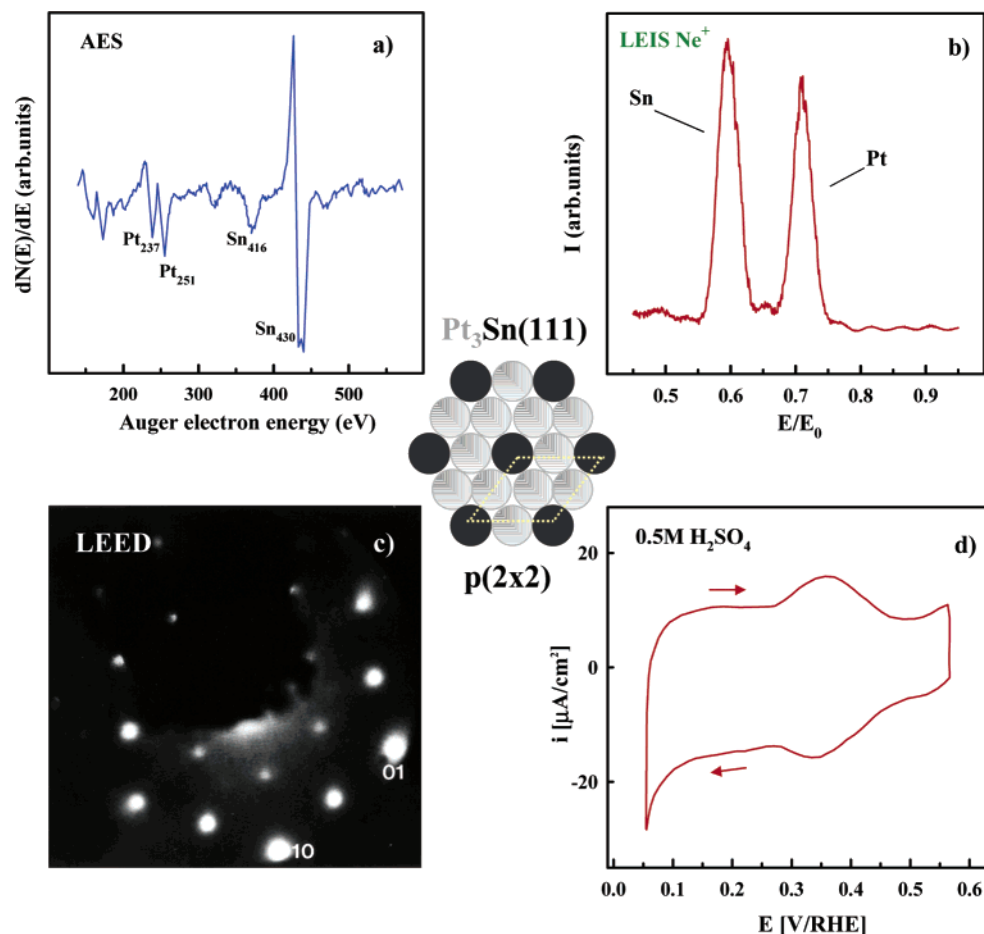


**Figure 1.** Surface characterization of the  $\text{Pt}_3\text{Sn}(111)$  in UHV: (a) AES, (b) LEIS and (c) LEED and (d) cyclic voltammetry in 0.5 M  $\text{H}_2\text{SO}_4$ , scan rate 50mV/s. Model is schematic representation of the observed  $p(2 \times 2)$  LEED pattern.

macroscopic level descriptions of the  $\text{Pt}_3\text{Sn}(111)$  surface in the electrochemical environment via atomic level characterization. First the structural properties of the  $\text{Pt}_3\text{Sn}(111)$  surface in electrolyte are examined by SXS, including both the stability of the UHV-prepared  $p(2 \times 2)$  structure in sulfuric acid solution and the potential-dependent relaxation of Pt and Sn atoms in the near-surface region. Adsorption of sulfuric acid anions on the  $p(2 \times 2)$  phase is examined by FTIR spectroscopy. These results unambiguously show that the puzzling pseudocapacitance in the cyclic voltammetry of  $\text{Pt}_3\text{Sn}(111)$  is associated with adsorption/desorption of (bi)sulfate anions on Pt sites. During electrochemical oxidation of CO on the  $p(2 \times 2)$  surface, in situ SXS and FTIR are used to show (explain) why  $\text{Pt}_3\text{Sn}(111)$  is so active for this reaction.

## 2. Experimental Section

The  $\text{Pt}_3\text{Sn}(111)$  single crystal was prepared by a procedure which has been fully described in refs 19 and 20, i.e., by combining high-purity platinum and tin in stoichiometric amounts and then refining the alloy using the Bridgman–Stockberger technique under a helium atmosphere in a high-purity alumina crucible. The composition of the intermetallic compound was confirmed by quantitative analysis using a wet chemical method and emission spectroscopy (Galbraith Laboratories) to be  $24.3 \pm 0.5\%$  Sn. Cylindrical single crystals oriented along (111), with a diameter of 6 mm and length of 4 mm, were cut by centerless grinding and then mechanically polished to  $0.05 \mu\text{m}$ . The

single crystal face was within  $0.1^\circ$  of its respective crystal plane as determined by Laue back reflection X-ray diffraction.

**2.1. UHV Surface Preparation and Characterization.** The  $\text{Pt}_3\text{Sn}(111)$  surface was prepared and characterized in a UHV system, with a base pressure of  $2 \times 10^{-10}$  Torr, equipped with an angular-resolving double pass cylindrical mirror analyzer (PHI-DPCMA  $\Phi 15$ -255GAR) with an electron source at its center. The surface was cleaned by repeated cycles of sputter-annealing until Auger electron spectroscopy (AES) indicated that a perfectly clean (carbon and oxygen free) surface was produced. AES spectra (Figure 1a) were recorded in derivative mode using the 3 keV electron beam energy, 3  $\text{eV}_{\text{p-p}}$  modulation, and  $-5 \mu\text{A}$  beam current in the range from 140 to 600 eV. The LEED pattern following  $\text{Ar}^+$  bombardment and annealing is shown in Figure 1c. In agreement with reference,<sup>21</sup> the clean-annealed surface produced half-order spots in the LEED pattern, characteristic of the  $p(2 \times 2)$  structure that is observed on other alloys having the same  $\text{Ll}_2$  structure as  $\text{Pt}_3\text{Sn}$ .<sup>22</sup> A real space model for the  $p(2 \times 2)$  surface is depicted in Figure 1. After mild sputtering (with a 0.5 keV beam of  $\text{Ar}^+$  ions) and annealing at 1000 K, the surface composition was determined by low-energy ion scattering (LEIS), see Figure 1b. LEIS spectra were taken with a  $\text{Ne}^+$  beam energy of 1 keV with sample current from 5 to 30 nA at residual Ne pressure of  $2.5 \times 10^{-8}$  Torr. The scattering angle was  $127^\circ$ , and the incidence angle was  $45^\circ$ . A  $\Phi 04$ -303A differentially pumped ion gun was used to raster the  $\text{Ne}^+$  ion beam over a  $3 \text{ mm} \times 3 \text{ mm}$  area. Using the theoretical ion-scattering cross-sections for Sn and Pt,<sup>23</sup> the LEIS spectrum indicates that the

(21) Haner, A. N.; Ross, P. N.; Bardi, U. *Surf. Sci.* **1991**, 249, 15–20.

(22) Ferrero, R.; Capelli, R.; Borsese, A.; Delfino, S. *Atti. Accad. Naz. Lincei Red. Cl. Sci. Fis. Mater. Nat.* **1973**, 54, 634.

(23) Taglauer, E.; Heiland, W. *Appl. Surf. Anal.* **1980**, 669, 111–124.

(20) Gasteiger, H. A.; Markovic, N. M.; Ross, P. N., Jr. *Catal. Lett.* **1996**, 36, 1–8.

surface composition is 25 at. % Sn and 75 at. % Pt, consistent with the  $p(2 \times 2)$  LEED pattern and bulk truncation of the surface structure.

**2.2. Electrochemical Measurements.** The UHV prepared and characterized  $Pt_3Sn(111)$  surface was transferred from the UHV introductory port (back-filled with argon) and covered immediately with a drop of triply pyro-distilled water, for details see ref 24. The electrode was then mounted in a rotating disk electrode and finally immersed in electrolyte under potential control at  $\sim 0.05$  V vs RHE in 0.5 M  $H_2SO_4$  (Baker, Ultrex). A typical cyclic voltammogram of the  $Pt_3Sn(111)$  in supporting electrolyte is shown in Figure 1d. The reference electrode was a saturated calomel electrode (SCE) separated by a bridge from the reference compartment. All potentials in this paper are, however, referenced to the potential of the reversible hydrogen electrode (RHE) at the same temperature (calibrated from the hydrogen oxidation reaction<sup>25</sup>) in the same electrolyte; argon was bubbled through a glass frit (Air Products, 5N8 purity). The geometrical surface area of the disk electrode was 0.283  $cm^2$ , and all voltammograms were recorded with a sweep rate of either 50 or 20 mV/s.

**2.3. FTIR Measurements.** The in situ FTIR measurements were taken with a Nicolet Nexus 670 spectrometer purged with nitrogen and equipped with a MCT detector cooled with liquid nitrogen. All IR measurements were performed in a spectroelectrochemical glass cell designed for an external reflection mode in a thin layer configuration. The cell is coupled at its bottom with a  $CaF_2$  prism beveled at  $60^\circ$  from the surface normal. Prior to each measurement, a cyclic voltammogram was recorded in order to confirm the cleanliness of the electrode surface. Subsequently the solution was saturated with CO for at least 3 min, holding the electrode potential at 0.05 V. The spectra were recorded with a resolution of 8  $cm^{-1}$ . All measurements were performed using p-polarized light. To obtain a single-beam spectrum, 50 scans were collected at each potential, resulting in a recording time of 25 s. Absorbance spectra were calculated as the ratio  $-\log(R/R_0)$ , where  $R$  and  $R_0$  are the reflectance values corresponding to the sample and reference spectra, respectively. Reference spectra were recorded either at 0.9 or +0.05 V, where  $CO_{ad}$  is completely oxidized and before the onset of  $CO_{ad}$  oxidation, respectively. The reference potential in the spectroelectrochemical cell was controlled by a RHE.

**2.4. SXS Measurements.** The general experimental procedure used in X-ray diffraction measurements of electrochemical systems has been described in detail in previous articles.<sup>4–6</sup> As for electrochemical measurements, the UHV prepared and characterized  $Pt_3Sn(111)$  crystal (miscut  $< 0.1^\circ$ ) was transferred into the X-ray electrochemical cell. The cell was mounted at the center of a four-circle Huber goniometer on beamline 7-2 at the Stanford Synchrotron Radiation Laboratory (SSRL), using a 10 keV X-ray beam, defined by slits to be a 1 mm  $\times$  1 mm spot at the sample. Diffracted X-rays were measured by a Ge solid-state detector after being passed through a Soller slit which defined an in-plane resolution of ca. 0.005  $\text{\AA}^{-1}$ . The crystal was indexed to the conventional hexagonal unit cell for the (111) surface. Further experimental details can be found in ref 26.

### 3. Results and Discussion

**3.1. Surface Characterization of  $Pt_3Sn(111)$ : LEED, CV, and SXS.** The ability to characterize atomic/molecular spatial structures and to monitor changes in the local symmetry of surface atoms in situ under reaction conditions has played an important part in surface electrochemistry at monocrystalline metal electrodes. For example, we used SXS to demonstrate that the  $(1 \times 1)$  surface of  $Pt(111)$ , prepared by a flame annealing method,<sup>27,28</sup> remains stable upon contact with aqueous

solutions or even when the potential is cycled between the hydrogen evolution and the oxide formation potential regions. There have been no studies, however, which could provide such links between the in situ surface structure/composition of bulk alloys and their adsorptive chemistry. As for  $Pt(111)$ , in the present work we have also used SXS to establish whether the  $p(2 \times 2)$  structure, observed by LEED in Figure 1c, remains stable in 0.5 M  $H_2SO_4$ . From the fact that upon contact with solution at 0.05 V the  $Pt_3Sn(111)$  surface remains flat and terminated by the bulk structure, we conclude the  $p(2 \times 2)$  structure of Sn can indeed be “transferred” from a UHV system to an electrochemical environment (!). Equally important, even when the electrode potential was cycled from hydrogen adsorption up to the 0.6 V, the  $p(2 \times 2)$  structure remained stable with the surface composition expected for the bulk termination surface structure (e.g., 25 at. % Sn). The important consequence of the structure/composition stability of  $Pt_3Sn(111)$  in 0.5 M  $H_2SO_4$  is that the interpretation of the cyclic voltammetry of  $Pt_3Sn(111)$  in argon-purged 0.5 M  $H_2SO_4$ , depicted in Figure 2a, can be based on the adsorption sites available on the  $p(2 \times 2)$  surface, see model in Figure 2. Notice that the  $H_{upd}$  pseudocapacitance ( $0.05 < E < \approx 0.25–0.35$  V) is considerably reduced from that of the corresponding Sn-free  $Pt(111)$  surface (see dotted curve in Figure 2a), as one might expect from an alloying element (Sn) that does not adsorb hydrogen.<sup>20</sup> Further inspection of Figure 2 clearly reveals that the  $H_{upd}$  potential region on  $Pt_3Sn(111)$  is followed with a puzzling reversible feature ( $0.25 < E < 0.5$  V) which could be produced by any number of processes including hydrogen adsorption, bisulfate adsorption, OH adsorption, and/or a Sn surface redox process.<sup>19</sup> In the next section, the nature of the “anomalous” feature in the cyclic voltammetry of  $Pt_3Sn(111)$  will be probed by means of FTIR spectroscopy.

**3.2. Bisulfate Adsorption on  $Pt_3Sn(111)$ : FTIR Measurements.** After more than two decades of controversy, it is now well established that the reversible “anomalous” feature observed in the CV of  $Pt(111)$  in sulfuric acid solutions between 0.35 and 0.65 V (Figure 2b) is due to adsorption/desorption of bisulfate anions. The first evidence was obtained from FTIR spectroscopy,<sup>9,11,12</sup> and then from radiotracer measurements,<sup>29,30</sup> chronocoulometric measurements,<sup>31a</sup> and finally STM experiments.<sup>31b</sup> As for the  $Pt(111)$ -bisulfate system, FTIR characterization of the  $Pt_3Sn(111)$  alloy in sulfuric acid solution is used to establish whether the origin of the “anomalous” feature in the voltammetry of Figure 2a also arises from bisulfate adsorption/desorption. Figure 2c shows sets of spectra obtained for the  $Pt_3Sn(111)$  alloy in 0.5 M  $H_2SO_4$  over the potential range from hydrogen evolution to just before the onset of Sn dissolution. A negative going band is clearly visible in the spectra at a potential near to the onset (ca. at 0.2 V) of the formation of the puzzling pseudocapacitance in Figure 2a. The band at low potentials is broad and weak with the peak position centered at ca. 1210  $cm^{-1}$ . As the potential is scanned positively, the band becomes more intense and at 0.5 V the peak position

(27) Clavilier, J. *J. Electroanal. Chem.* **1980**, *107*, 211–216.

(28) Markovic, N. M.; Hanson, M.; McDougal, G.; Yeager, E. *J. Electroanal. Chem.* **1986**, *241*, 309.

(29) Zelenay, P.; Wieckowski, A. *J. Electrochem. Soc.* **1992**, *139*, 2552–2558.

(30) Kolics, A.; Wieckowski, A. *J. Phys. Chem. B* **2001**, *105*, 2588–2595.

(31) (a) Savich, W.; Sun, S. G.; Lipkowski, J.; Wieckowski, A. *J. Electroanal. Chem.* **1995**, *388*, 233–237. (b) Funtikov, A. M.; Stimming, U.; Vogel, R. *J. Electroanal. Chem.* **1997**, *482*, 147–153.

(24) Gasteiger, H. A.; Markovic, N.; Ross, P. N.; Cairns, E. J. *J. Phys. Chem.* **1993**, *97*, 12020–12029.

(25) Markovic, N. M.; Grgur, B. N.; Ross, P. N., Jr. *J. Phys. Chem. B* **1997**, *101*, 5405–5413.

(26) Lucas, C. A.; Markovic, N. M.; Grgur, B. N.; Ross, P. N., Jr. *Surf. Sci.* **2000**, *448*, 65–76.

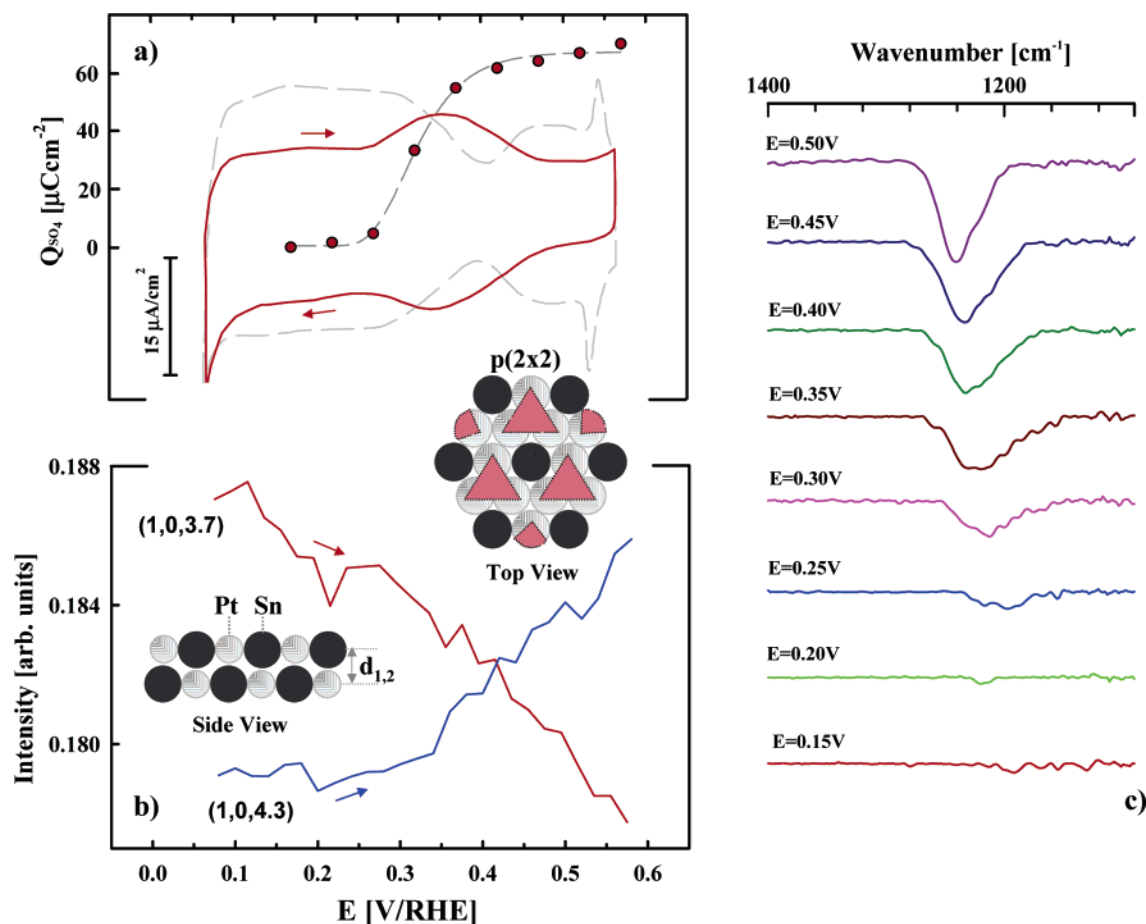


**Figure 2.** (a) Cyclic voltammograms of Pt(111) (dashed gray line) and Pt<sub>3</sub>Sn(111) (solid red line) in 0.5 M H<sub>2</sub>SO<sub>4</sub>, scan rate 50 mV/s. Potential-dependent integrated charges for the adsorption of (bi)sulfate anions on the Pt<sub>3</sub>Sn(111) surface are represented by circles. (b) The measured X-ray intensities at (1, 0, 3.7) and (1, 0, 4.3) as a function of the electrode potential. Top and side views represent the proposed  $p(2 \times 2)$  structure. The gray circles are Pt surface atoms, the black circles are Sn atoms, and triangles are (bi)sulfate anions which are adsorbed on Pt sites. The side view indicates the surface normal spacing that is derived from the CTR measurements. (c) IRAS spectra of (bi)sulfate anions adsorbed at Pt<sub>3</sub>Sn(111) recorded as the potential was stepped in sequence from -0.05 to 0.65 V.

shifts to ca.  $1240\text{ cm}^{-1}$ . Interestingly, very similar FTIR spectra have been recorded for the adsorption of (bi)sulfate<sup>32</sup> anions on Pt(111).<sup>9</sup> This similarity is not coincidental and can be used as confirmation that the “anomalous” feature observed in the CV of Pt<sub>3</sub>Sn(111) corresponds to (bi)sulfate anion adsorption at Pt sites. The recognition that FTIR spectra for bisulfate adsorption on Pt(111) in ref 9 are almost identical with those depicted in Figure 2c also suggests that Sn atoms have only a small effect on the active Pt–(bi)sulfate bands. The potential-dependent surface coverage of (bi)sulfate anions on the Pt<sub>3</sub>Sn(111) surface, obtained by integrating the charge under the pseudo-capacitance between 0.2 and 0.5 V, is plotted in Figure 2a. The total charge passing the interface in this potential region is ca.  $65\ \mu\text{C}/\text{cm}^2$ , or about 75% of that of the corresponding Sn-free Pt(111) surface ( $\approx 80\ \mu\text{C}/\text{cm}^2$ ). Thus, the charge for the (bi)sulfate

adsorption on the former surface is reduced by  $\approx 25\%$  from the charge required to form a close-packed layer of (bi)sulfate anions on the Pt(111) surface, or simply by the amount of Sn atoms present in the  $p(2 \times 2)$  structure. This suggests that (bi)sulfate anions are not adsorbed on Sn atoms. A representation of a possible structural model for (bi)sulfate adsorption on the  $p(2 \times 2)$  Pt<sub>3</sub>Sn(111) surface is depicted in Figure 2. On the basis of this model, a tetrahedral (bi)sulfate anion is adsorbed on Pt atoms via the three oxygen atoms, as proposed for the (bi)sulfate interaction with the Pt(111) surface.<sup>33</sup>

Further inspection of Figure 2a reveals that adsorption of (bi)sulfate anions on Pt<sub>3</sub>Sn(111) takes place at more negative potentials than on Pt(111), ca. 0.15 V. An enhancement of anion adsorption on Pt(111) modified with admetals is not surprising and it has been observed previously in radiotracer work by Wieckowski and co-workers for the Pt–Cu<sub>upd</sub> system,<sup>34</sup> by Lipkowski and co-workers for the Au(111)–Cu<sub>upd</sub> systems,<sup>35,36</sup> and by our group for the Pt–Cu<sub>upd</sub>,<sup>37,38</sup> Pt–Pb<sub>upd</sub>,<sup>39</sup> and Pt–

(32) For the Pt(111)–bisulfate system, there has been some controversy about the assignment of the adsorbed bands for sulfuric acid anion. Initially, Faguy et al. assigned this band to an SO<sub>3</sub> asymmetric stretching mode of bisulfate anions which are adsorbed on the Pt atoms via the three unprotonated oxygen atoms. Subsequent studies by other groups have disputed this interpretation and the same band was assigned to a symmetric SO<sub>3</sub> stretch of bisulfate anions<sup>10,11</sup> or to the S–O stretch of noncoordinated SO group of the adsorbed sulfate anion.<sup>12</sup> To reconcile these two extremes, Faguy et al. recently suggested that the adsorbate in the anomalous potential region is a H<sub>3</sub>O<sup>+</sup>–SO<sub>4</sub><sup>2-</sup> species.<sup>70</sup> We consider the issue unresolved and thus refer to adsorbing species on Pt(111) in the “butterfly” region equivocally as (bi)sulfate.

(33) Markovic, N. M.; Marinkovic, N. S.; Adzic, R. R. *J. Electroanal. Chem.* **1988**, *241*, 309.

(34) Varga, P.; Zelenay, P.; Wieckowski, A. *J. Electroanal. Chem.* **1992**, *330*, 453–467.

(35) Shi, Z.; Lipkowski, J. *J. Electroanal. Chem.* **1994**, *364*, 289–294.

(36) Wu, S.; Shi, Z.; Lipkowski, J.; Hitchcock, A. P.; Tyliczszak, T. *J. Phys. Chem.* **1997**, *103100*–10322.

(37) Markovic, N.; Ross, P. N. *Langmuir* **1993**, *9*, 580–590.

$\text{Bi}_{\text{upd}}^{40}$  systems. We suggested a mechanism for this induced anion adsorption in terms of the local work function concept and the local pzc effect.<sup>41</sup> These concepts have been discussed previously,<sup>39,40,42,43</sup> so the remarks here are correspondingly brief. Modifying Pt with Cu and Pb adatoms lowers the work function of Pt atoms within a Fermi–Thomas screening length of the admetal, resulting in more anion adsorption at these sites at the given electrode potential than on the sites which are not affected by the UPD adatoms. Using the same argument for the Pt–Sn system, adsorption of (bi)sulfate anions on the  $\text{Pt}_3\text{Sn}(111)$  surface is observed at a lower electrode potential than on an unmodified Pt(111) surface because Sn lowers the work function of the Pt atoms.

**3.3. Adsorbate-Induced Structural Changes.** Having established the potential window of stability of the  $p(2 \times 2)$  structure in electrolyte, additional structure details, such as adsorbate induced surface relaxation, were examined by analyzing crystal truncation rods (CTR: CTR are rods of scattering which are aligned along the surface normal in the  $\text{Pt}_3\text{Sn}(111)$  reciprocal space and pass through bulk Bragg reflections.<sup>44</sup>) data.<sup>1–3,44</sup> A detailed examination of the CTR data will be presented in our next paper. Selected results from that study are given here in order to provide a complete picture of the  $\text{Pt}_3\text{Sn}(111)$  surface in electrolyte under reaction conditions. Figure 2b shows results from the measurements of X-ray intensity changes at (1, 0, 3.7) and (1, 0, 4.3) reciprocal lattice points, i.e., where the scattered intensity is sensitive to surface relaxation effects. Since scattering from  $\text{H}_{\text{upd}}$ ,  $\text{OH}_{\text{ad}}$ , and (bi)sulfate anions makes a negligible contribution relative to the diffraction from the topmost Pt and Sn atoms, the crystal truncation rods reflect adsorbate-induced changes in the Pt (Sn) surface normal structure (the interplanar spacing ( $\Delta d_{1,2}$ ) in Figure 2b). This method of measuring the potential dependence of the  $\text{Pt}_3\text{Sn}(111)$  surface relaxation will hereafter be referred to as X-ray voltammetry, XRV.<sup>45a</sup> The fact that the X-ray intensities at these two reciprocal lattice points show “mirror-like” behavior as the potential is scanned is consistent with a surface relaxation effect rather than surface roughening. Close inspection of the XRV results in Figure 2b reveals that the desorption of hydrogen as well as the adsorption of bisulfate anions lead to contraction of the surface atoms, i.e.,  $\Delta d_{1,2}$  interplanar spacing in the inset of Figure 2b decreases monotonically by scanning the potential positively from 0.05 V. In line with previous studies,<sup>4</sup> analysis of the relevant CTR data has been performed in order to extract the detailed structural parameters for the  $\text{Pt}_3\text{Sn}(111)$  surface in electrolyte. From fits of the CTR data, i.e., using a structural model in which the vertical displacement ( $\Delta d_{\text{Pt}}$ ,  $\Delta d_{\text{Sn}}$ ), surface coverage ( $\Theta_{\text{Pt}}$ ,  $\Theta_{\text{Sn}}$ ), and roughness ( $\sigma_{\text{Pt}}$ ,  $\sigma_{\text{Sn}}$ ) of the Pt and Sn in the topmost two layers were allowed to vary independently, the results indicated

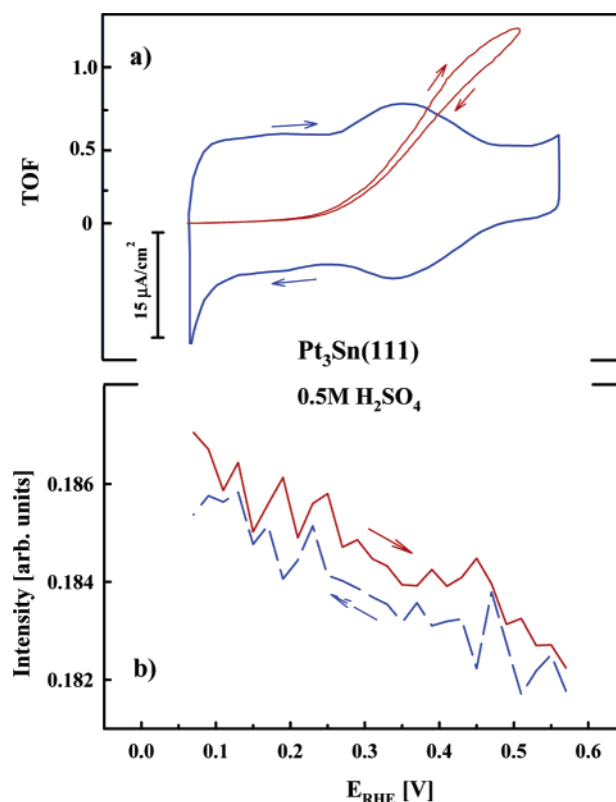


**Figure 3.** (a) Cyclic voltammogram of the  $\text{Pt}_3\text{Sn}(111)$  in 0.5 M  $\text{H}_2\text{SO}_4$  and corresponding polarization curve for the CO oxidation dissolved (1atm) in solution, scan rate 50 mV/s. The kinetics of CO oxidation in CO saturated solution is expressed by the turn over frequency (TOF), defined as the number of complete reaction events per active sites per second, i.e.,  $\text{TOF} = i/nFN$ , where  $i$  is the measured current density and  $N$  is the density of active sites. (b) The measured X-ray intensities at (1, 0, 3.7) as a function of the electrode potentials in 0.5 M  $\text{H}_2\text{SO}_4$  saturated with CO.

two important characteristics of the surface structure at 0.05 and 0.55 V: (i) at 0.05 V expansion of the surface Pt atoms induced by the adsorption of hydrogen is very similar to that observed on Pt(111)<sup>45</sup> ( $\Delta d_{\text{Pt}}^1 = +2\%$ ); (ii) at 0.55 V the  $p(2 \times 2)$  structure remains stable but, while the Pt surface atoms are unrelaxed, the Sn atoms in the topmost layer expand up to  $\Delta d_{\text{Pt}}^1 = 8.5\%$  of the lattice spacing. At potentials higher than 0.55 V, this expansion is even more pronounced, indicating that before Sn dissolution the Sn surface atoms are expanded by ca. 12% of the bulk lattice spacing.

**3.4. CO Oxidation on  $\text{Pt}_3\text{Sn}(111)$ : Surface Structures under Reaction Conditions.** The electrooxidation of CO on  $\text{Pt}_3\text{Sn}(hkl)$  surfaces occupies an important position in surface electrochemistry. Concentrating on both catalytic activity and structure sensitivity, Gasteiger et al. demonstrated that  $\text{Pt}_3\text{Sn}(hkl)$  single crystals have one of the highest catalytic activity for CO oxidation ever found at the metal–liquid interface in acid solutions.<sup>20</sup> The most active surface was found to be  $\text{Pt}_3\text{Sn}(111)$ , an alloy on which the onset potential for the continuous oxidation of dissolved CO (ca. 0.2 V in Figure 3a) is shifted negatively with respect to that for the  $\text{Pt}_3\text{Sn}(110)$  surface by about 0.1 V and by  $\approx 0.45$  V with respect to pure Pt. It was proposed that the significant enhancement produced by alloying Pt with Sn atoms can be ascribed to a combination of both bifunctional and ligand (electronic) effects.<sup>19,20</sup>

In the bifunctional effect, Sn nucleates oxygenated species<sup>46</sup> which then react with the adsorbed CO (hereafter denoted as

(38) Markovic, N.; Gasteiger, H. A.; Ross, P. N. *Langmuir* **1995**, *11*, 4098–4108.

(39) Markovic, N. M.; Grgur, B. N.; Lucas, C.; Ross, P. N. *J. Chem. Soc., Faraday Trans.* **1998**, *94*, 3373–3379.

(40) Schmidt, T. J.; Stamenkovic, V.; Lucas, C.; Markovic, N. M.; Ross, P. N. *Phys. Chem. Chem. Phys.* **2001**, *3*, 3879–3890.

(41) Markovic, N. M.; Ross, P. N. *J. Electroanal. Chem.* **1992**, *330*, 499–520.

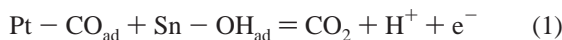
(42) Schmidt, T. J.; Grgur, B. N.; Behm, R. J.; Markovic, N. M.; Ross, P. N., Jr. *Phys. Chem. Chem. Phys.* **2000**, *2*, 4379–4386.

(43) Stamenkovic, V.; Markovic, N. M. *Langmuir* **2000**, *17*, 2388–2394.

(44) Feidenhans'l, R. *Surf. Sci. Rep.* **1989**, *10*, 105–188.

(45) (a) Lucas, C. A.; Markovic, N. M.; Ross, P. N. *Surf. Sci.* **1999**, *425*, L381–L386. (b) Tidswell, I. M.; Markovic, N. M.; Ross, P. N. *J. Electroanal. Chem.* **1994**, *376*, 119–126.

CO<sub>ad</sub>) on Pt atoms,<sup>20</sup>



This mechanism is consistent with the positive reaction order with respect to the partial pressure of dissolved CO (hereafter denoted as CO<sub>b</sub>). In agreement with experimental observations, from the calculated binding energies of CO and OH on the Pt<sub>3</sub>Sn(111) surface it was found that while CO does not bind to the Sn, OH<sub>ad</sub> clearly shows a preference for the Sn atop coordination surface atoms.<sup>47</sup> On the other hand, the ligand effect, where the second component (Sn atoms) may alter the electronic properties of catalytically active metal (Pt atoms), is a consequence of the strong intermetallic bonding between Pt and Sn. The ligand effect is multifaceted, including the formation of the so-called “weakly” adsorbed state of CO<sub>ad</sub><sup>20,48</sup> (denoted as CO<sub>ad</sub><sup>w</sup>) on Pt sites as well as an increased stability of Sn atoms in the Pt<sub>3</sub>Sn surface.<sup>20</sup> Due to lack of any atomic-level structure information in our early work, we could only characterize the CO<sub>ad</sub><sup>w</sup> state thermodynamically, i.e., CO<sub>ad</sub>, with a low heat of adsorption. In what follows, by a combination of SXS and FTIR measurements, this macroscopic description of the CO<sub>ad</sub><sup>w</sup> state will be elevated to a microscopic level, which enables the relation between reactivity and the interfacial structure of CO<sub>ad</sub> on Pt<sub>3</sub>Sn(111) to be understood.

**3.4.1. SXS Measurements.** Direct information regarding the CO<sub>ad</sub> structure and stability of the p(2 × 2) phase in the presence of CO<sub>b</sub> was established by using SXS. The p(2 × 2) structure remains stable in a solution containing CO, and the potential window of stability appears to be even wider than in CO-free solution, i.e., between 0.05 < E < 0.9 V. As a consequence, the polarization curve for CO oxidation, shown in Figure 2a, corresponds to CO<sub>ad</sub> oxidation on a well-ordered Pt<sub>3</sub>Sn(111) surface. Unfortunately, in contrast to the Pt(111)–CO system<sup>45a,48</sup> it was not possible to detect ordered structures of CO on the Pt<sub>3</sub>Sn(111) surface by SXS.

The expansion of surface atoms upon the adsorption of CO on the Pt<sub>3</sub>Sn(111) surface (CO is exclusively adsorbed on Pt sites<sup>20</sup>) is ca. 1.5%, which is significantly smaller than the ca. 4% expansion induced by the adsorption of CO on Pt(111).<sup>45a,49</sup> The difference in relaxation of Pt(111) and Pt<sub>3</sub>Sn(111) surface layers covered with CO most likely arises from the difference in the adsorbate–metal bonding, the Pt(111)–CO interaction being stronger than the Pt<sub>3</sub>Sn(111)–CO. This observation provides a first independent confirmation of the existence of the “weakly” adsorbed state of CO on the Pt<sub>3</sub>Sn(111) surface, originally proposed by our group<sup>20</sup> and later supported by density functional theory (DFT) calculations.<sup>47</sup> The DFT calculations indicated that on Pt<sub>3</sub>Sn(111) CO binds only to Pt atoms (with binding energy of –1.20 eV vs –1.41 eV for the pure Pt) and not to the Sn atom, whereas OH has an energetic preference for the Sn sites (with binding energy of –2.66 eV).

Direct information regarding the induced relaxation of surface Pt and Sn atoms by the adsorption of CO are obtained by analyzing and modeling CTR data (not shown). Those results for the Pt<sub>3</sub>Sn(111)–CO system indicated that the measurements were insensitive to both the CO adlayer (formed on Pt ensembles of the p(2 × 2) structure) and the oxygenated species (present on Sn atoms) due to the relatively weak scattering power of C, O, and H atoms compared to Pt and Sn atoms. Using the same structural model used to describe the Pt<sub>3</sub>Sn(111) surface in the absence of CO, general conclusions obtained from modeling CTR data can be summarized as follows: while at 0.05 V both Pt and Sn atoms are expanded relatively little from the bulk lattice spacing (ca. 1.5%), at 0.5 V the expansion of Pt atoms remains the same as at low potentials, in contrast to significant expansion of the Sn atoms from the second layer, ca. 6%. Although Sn atoms are highly expanded from the bulk lattice position, the XRV in Figure 3b shows that upon sweeping the potential positively from 0.05 V the oxidation of CO is associated with a net contraction of the surface layer, consistent with our previous remarks that the relaxation of the topmost layer at positive potentials is predominantly controlled by the contraction of the majority Pt rich (75 at. %) surface atoms.

**3.4.2. FTIR measurements.** The binding site occupancy of CO on the Pt<sub>3</sub>Sn(111) surface was obtained by utilizing FTIR spectroscopy, shown previously for the interaction of CO with the Pt(111) surface.<sup>49</sup> Figure 4b shows a set of the CO absorbance spectra referenced to the single-beam spectrum collected at 0.65 V. The assignment of CO adsorption sites on Pt<sub>3</sub>Sn(111) can best be done by comparing the present data to those from the system Pt(111)–CO<sub>ad</sub>, the latter being described in detail by many groups.<sup>50–53</sup> From Figure 4b and references,<sup>49,51</sup> therefore, it is clear that at low overpotentials (0.05 < E < 0.2 V) an a-top/3-fold-hollow combination of CO<sub>ad</sub>, which are characteristic for the Pt(111)–CO system, is not observed at the Pt<sub>3</sub>Sn(111) surface. In addition, in contrast to the near invariant bands of a-top CO on Pt(111),<sup>49</sup> changes in the band shape (splitting of the band) and frequency are clearly visible on the Pt<sub>3</sub>Sn(111) surface in the same potential range. Further inspection of Figure 4b indicates that a pair of bands centered at ca. 2090 and 2077 cm<sup>–1</sup> (at low potentials) are transformed into a single relatively broad peak centered at ca. 2077 cm<sup>–1</sup> at higher potentials. While the terminal feature is of central concern here, the properties of the bridge CO IR band are also of interest, especially since comparison of these features sheds light on the differences between the Pt(111)–CO<sub>ad</sub> and Pt<sub>3</sub>Sn(111)–CO<sub>ad</sub> systems. Figure 4a shows that characteristic C–O stretching bands near 1826–1842 cm<sup>–1</sup>, corresponding to the bridge-bonded CO, appear in spectra at potentials above 0.25 V. As we shall see in section 3.6, in time-resolved experiments the bridge-bonded CO may even be observed at 0.1 V. Notice that on the Pt(111) electrode an atop/bridge combination in acid solutions is observed at much higher potentials (E > 0.4 V), implying that the oxidation of CO at E < 0.2 V (production of CO<sub>2</sub> in Figure 4a) reduces the surface coverage of CO at the Pt<sub>3</sub>Sn(111) surface and thus the a-top/bridge combination, characteristic for the Pt(111)–CO system,

(46) As discussed below, the true nature of oxygenated species adsorbed on Sn is still unknown, e.g., Sn atoms in the Pt–Sn alloy may have multiple oxygenated ligands, the stoichiometry of which may vary with the potential. For the sake of simplicity, however, in the further discussion these oxygenated species will simply be assigned as OH<sub>ad</sub>.

(47) Shubina, T. E.; Koper, M. T. M. *Electrochim. Acta* **2002**, *47*, 3621–3628.

(48) Markovic, N. M.; Grgur, B. N.; Lucas, C. A.; Ross, P. N. *J. Phys. Chem. B* **1999**, *103*, 487–495.

(49) Markovic, N. M.; Lucas, C. A.; Rodes, A.; Stamenkovic, V.; Ross, P. N. *Surf. Sci. Lett.* **2002**, *499*, L149–L158.

(50) Kitamura, T.; Takahashi, M.; Ito, M. *Surf. Sci.* **1989**, *358*, 337.

(51) Villegas, I.; Weaver, M. J. *J. Chem. Phys.* **1994**, *101*, 1648.

(52) Iwasita, T.; Nart, F. C. *Prog. Surf. Sci.* **1997**, *55*, 271–340.

(53) Rodes, A.; Gomez, R.; Feliu, J. M.; Weaver, M. J. *Langmuir* **2001**, *16*, 811–816.

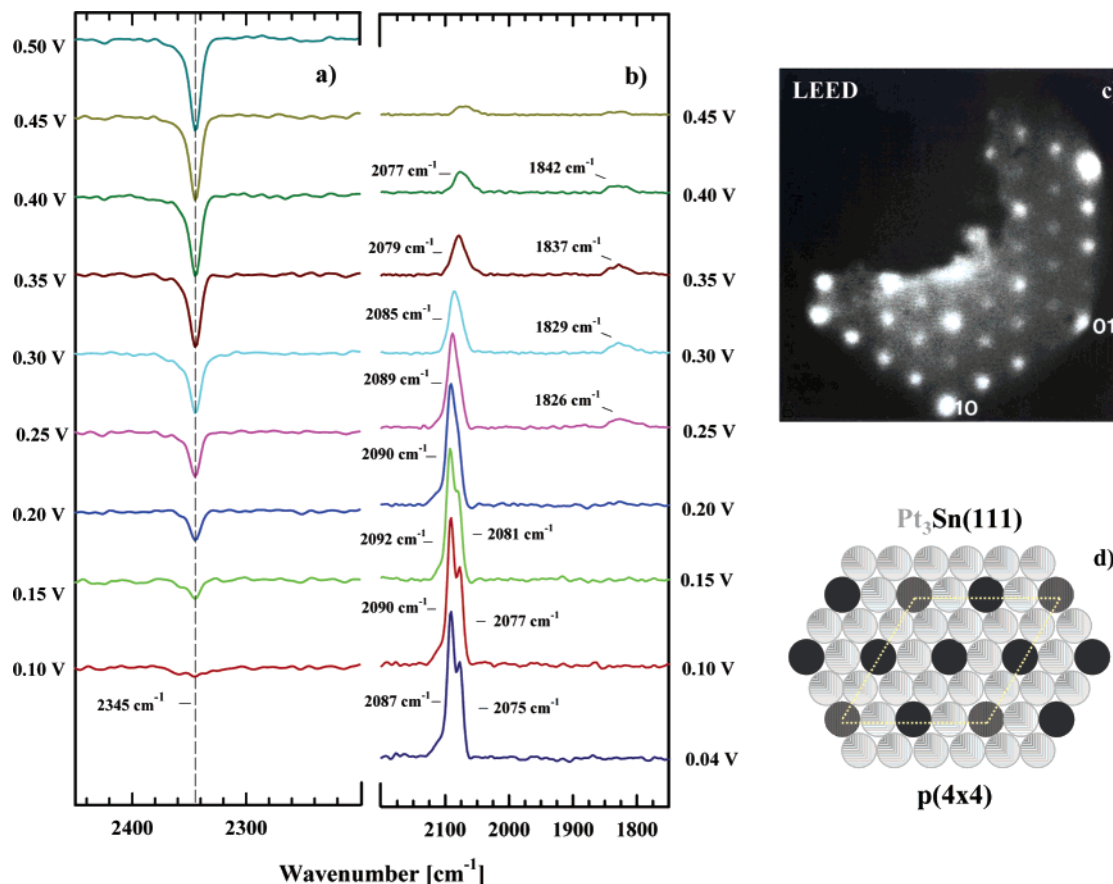


**Figure 4.** Series of infrared spectra during (a) CO<sub>2</sub> production and (b) progressive oxidation of CO on Pt<sub>3</sub>Sn(111) in 0.5 M H<sub>2</sub>SO<sub>4</sub> saturated with CO; each spectrum is accumulated from 50 interferometer scans at the potential indicated. (c) LEED pattern and (d) schematic representation of the p(4 × 4) structure observed on Pt<sub>3</sub>Sn(111) after exposing surface to O<sub>2</sub>. The gray circles are Pt surface atoms, the black circles are Sn atoms covered with OH, and the dashed circles are Sn atoms which are chemically different from Sn atoms modified with OH.

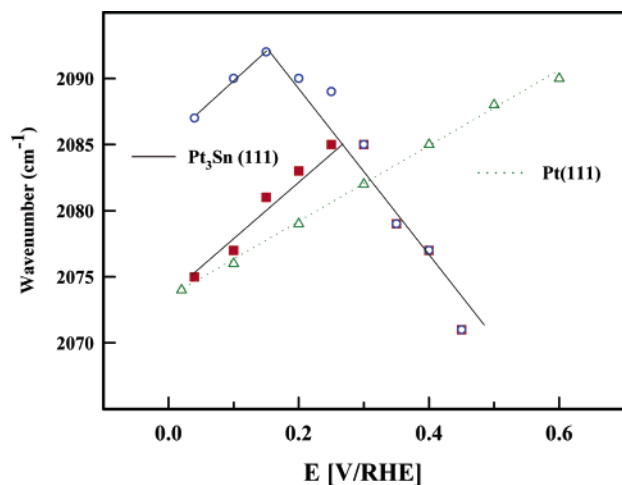


**Figure 5.** Plots of the peak frequency for the linear CO band vs the electrode potential on (triangles) Pt(111) and (open circles and squares) Pt<sub>3</sub>Sn(111) in 0.5 M H<sub>2</sub>SO<sub>4</sub>. Data obtained from Figure 4.

appears at much lower potentials. Essentially equivalent results for the CO binding site occupancy were obtained for the Pt(111)–CO system in alkaline solution,<sup>49</sup> except that an a-top/3-fold-hollow combination of CO<sub>ad</sub> is observed at  $E < 0.2$  V.

An illustrative example of the observed differences between CO<sub>ad</sub> adlayers on Pt(111) and Pt<sub>3</sub>Sn(111) is shown in Figure 5, which is a plot of the a-top stretching frequency ( $\nu$ ) versus the electrode potential. As shown previously,<sup>54</sup> on Pt(111) the linear

$\nu_{\text{CO}}-E$  plot, with a slope of ca. 30 cm<sup>-1</sup> V<sup>-1</sup>, is seen prior to occurrence of significant CO oxidation ( $E > 0.6$  V). On Pt<sub>3</sub>Sn(111), however, the  $\nu_{\text{CO}}-E$  slopes for both the high-frequency and low-frequency CO increase substantially, being ca. 45 cm<sup>-1</sup> V<sup>-1</sup> in the potential region just before CO oxidation starts ( $E > 0.2$  V). Observations of the potential effect on the band center in electrochemical experiments are described with equal validity as a change in the extent of d $\pi^*$  metal–CO back-bonding<sup>55,56</sup> with applied potential or from a shift of the vibrational frequency from the static electric field of the double layer, the so-called electrochemical Stark effect.<sup>57</sup> It is interesting that the potential-dependent behavior of the a-top  $\nu_{\text{CO}}$  feature illustrated in Figure 5 may be comparable to the coverage-dependent dipole coupling for CO adsorbed at Pt(111) in 0.1 M HClO<sub>4</sub> previously discussed by Chang and Weaver.<sup>54</sup> The latter results indicated that the  $d\nu_{\text{CO}}/dE$  slopes for the a-top CO increase with decreasing coverage with CO<sub>ad</sub>. Along the same lines, and considering that CO is *not* adsorbed on Sn atoms, the large Stark tuning slope on Pt<sub>3</sub>Sn(111) is consistent with the CO<sub>ad</sub> adlayer having a lower overall density on this surface than on Pt(111). It appears, therefore, that the surface Sn atoms cause the CO patches to be separated, which would weaken the vibrational coupling between patches and give rise to the observed large Stark tuning slope (45 cm<sup>-1</sup> V<sup>-1</sup>).

(54) Chang, S. C.; Weaver, M. J. *J. Chem. Phys.* **1990**, 4582–4594.

(55) Holloway, S.; Norskov, J. K. *J. Electroanal. Chem.* **1984**, 101, 193.

(56) Anderson, A. B. *J. Electroanal. Chem.* **1990**, 280, 37.

(57) Lambert, D. K. *Electrochim. Acta* **1995**, 41, 623–630.

Nevertheless, regardless of the exact explanation for how  $\nu_{\text{CO}}$  depends on  $E$ , it is reasonable to assume that the  $\nu_{\text{CO}}-E$  slopes in an electrochemical environment are dependent on the electrostatic parameters controlled by the applied potential as well as on the substrate-CO energetics. Although there is no straightforward correlation between the C-O stretching frequency and binding energy,<sup>58</sup> the appearance of the higher frequency mode of CO on Pt<sub>3</sub>Sn(111) may indicate the formation of a compressed CO adlayer. This layer due to chemical interaction between Pt and Sn atoms (e.g., alloying effects attributed to back-donation of metal electrons into antibonding CO orbitals, which stabilizes the metal-molecule bond and weaker the C-O bond) may lead to the formation of high density patches of CO and hence the weakly adsorbed state of CO on Pt sites. Recall that this is in accord with the DFT calculations.<sup>47</sup> In contrast to DFT calculations, however, the most stable adsorption site for CO on the Pt<sub>3</sub>Sn(111) surface are the a-top sites. The DFT calculations indicate a preference for the hollow hcp 3-fold sites with the Sn atom in the second layer; these sites are preferred over the a-top site by ca. 0.41 eV. Clearly, the alloying effect alone, which was taken into account in the DFT calculations, cannot accurately predict the potential-induced band shape/frequency behavior observed for the CO adlayer on the Pt<sub>3</sub>Sn(111) surface. Other factors, such as CO compression into smaller islands, which is governed by intermolecular repulsion, should be taken into account to explain the results in Figure 4b. The phenomenon of island compression is observed in segregated systems where the presence of one species causes the other species to segregate into patches in which the local density is higher than that observed when an equivalent amount of particular species is adsorbed alone.<sup>59</sup> Extending this phenomenon to Figure 4, the presence of oxygenated species on Sn may lead to compression of CO<sub>ad</sub> molecules resulting in higher local CO coverage that would yield blue-shifted CO frequencies from the enhanced dipole-dipole coupling. Model calculations indicate that only very small clusters (ca. 10 molecules) would be required in order to account for the observed high frequencies on the basis of dipole-dipole coupling.<sup>60</sup> For the Pt<sub>3</sub>Sn(111)-CO system, the compressive forces can be attributed to the repulsive CO<sub>ad</sub>-OH<sub>ad</sub> interaction. The existence of a repulsive CO-O interaction and compression of coadsorbed CO and O into islands on Pt single crystal surfaces are well established in UHV experiments and have been discussed independently by Engel and Ertl<sup>61</sup> and White.<sup>59</sup>

Although the proposition that the high-frequency band is a consequence of mutual interactions between CO<sub>ad</sub> and OH<sub>ad</sub> sounds reasonable, it is still puzzling as to why on a monoenergetic surface two kinds of CO islands can be formed. In general, at the metal-liquid interface the splitting of CO vibrational bands is a fairly universal phenomenon: e.g., adsorption of CO on Pt stepped single-crystal surfaces covered by submonolayer of CO,<sup>62-64</sup> some bimetallic surfaces at which

CO is adsorbed on *both* components<sup>65,66</sup> and on more oxophilic metals than Pt, e.g., on a Rh electrode<sup>67</sup> and the Pd(111) surface.<sup>68</sup> Given that SXS results have unambiguously showed that the Pt<sub>3</sub>Sn(111) surface is well-ordered and based on the fact that CO is not adsorbed on Sn, one can exclude the first two explanations. Another possible explanation is that Sn exists in two different oxidation states on the Pt<sub>3</sub>Sn(111) surface. The hypothesis would be that CO<sub>ad</sub> adsorbed next to each Sn site would have a unique frequency and potential dependence.

**3.5. Oxidation States of Sn: Ex Situ LEED/AES.** Neither the nature of oxygenated species nor its coverage on Sn atoms is known, and none of the in situ spectroscopic techniques we employed were able to resolve this issue. We decided therefore to return to the ex situ approach, hoping to obtain in UHV information about the “oxide” formation of Sn atoms. In the UHV experiments, the Pt<sub>3</sub>Sn(111) surface was exposed to oxygen and the corresponding structure/chemical changes were monitored by LEED/AES. Dosing the clean annealed surface with oxygen up to  $4 \times 10^{-8}$  Torr and at 300 °C produced a sharp p(4 × 4) pattern (Figure 4c) with a Sn/Pt AES ratio of 4.8 (slightly higher than the AES ratio of 4.5 for the p(2 × 2) pattern). These results indicate that chemisorption of oxygen occurs without changing the underlying structure or composition in the Pt<sub>3</sub>Sn(111) alloy surface, consistent with in situ SXS measurements. The fact that the adsorbed oxygen could only be desorbed by flashing the crystal to 700 °C (ca. 100 °C higher than for pure Pt) suggests that for the dosing conditions employed in our experiments the oxygen was adsorbed selectively onto Sn sites on the surface. Therefore, the p(4 × 4) LEED pattern could be interpreted as the adsorption on an oxygen adatom on every other Sn surface atom, as illustrated schematically in Figure 4d.

In what follows, we apply the oxidation results in UHV to an electrochemical environment, assuming that even in electrolyte not every Sn atom is covered with oxygenated species (or at least not with the same-kind of oxygenated species). For simplicity, however, we consider that OH is selectively adsorbed on every second atom and OH-free atoms will be assigned as “non-oxidized” Sn atoms. Under these circumstances, while the high-frequency CO<sub>ad</sub> may occupy Pt atoms which are adjacent to “OH<sub>ad</sub>”-covered Sn atoms (black circles in the model of Figure 4d), the low-frequency CO may occupy Pt sites in the vicinity of “non-oxidized” Sn atoms (shaded circles in the model of Figure 4d). Recall that in the former case the repulsive CO<sub>ad</sub>-OH<sub>ad</sub> interaction leads to formation of cluster domains where the local CO coverage within such patches remains higher than in the latter case.

**3.6. Time-Resolved FTIR Spectroscopy of CO Oxidation.** Figures 6a and 6b show that the oxidative removal of CO<sub>ad</sub> from the Pt<sub>3</sub>Sn(111) surface, established by monitoring the concomitant development of the asymmetric O-C-O stretch of dissolved CO<sub>2</sub> at 2343 cm<sup>-1</sup>, starts at as low as 0.1 V. Plots of the integrated intensities of the adsorbed CO stretching band ( $I_{\text{CO}}$ ) and the integrated intensities for CO<sub>2</sub> production ( $I_{\text{CO}_2}$ ) as a function of electrode potential in CO saturated 0.5 M H<sub>2</sub>SO<sub>4</sub>

(58) Koper, M.; van Santen, R. A.; Wasilewski, S. A.; Weaver, M. J. *J. Chem. Phys.* **2000**, *113*, 4392-4407.

(59) White J. M.; Akhter, S. *Critical Reviews in Solid State Materials Science*; CRC: Boca Raton, FL, 1988; pp 131-173.

(60) Severson, M. W.; Stuhlmann, C.; Villegas, I.; Weaver, M. J. *J. Chem. Phys.* **1995**, *103*, 9832-9843.

(61) Engel, T.; Ertl, G. *Adv. Catal.* **1979**, *28*, 1.

(62) Kim, C. S.; Korzeniewski, C.; Tornquist, W. J. *J. Chem. Phys.* **1993**, *100*, 628-630.

(63) Kim, C. S.; Tornquist, W. J.; Korzeniewski, C. *J. Chem. Phys.* **1994**, *101*, 9113-9121.

(64) Kim, C. S.; Korzeniewski, C. *Anal. Chem.* **1997**, *69*, 2349-2353.

(65) Friedrich, K. A.; Geyzers, K.-P.; Linke, U.; Stimming, U.; Stumper, J. *J. Electroanal. Chem.* **1996**, *402*, 123-128.

(66) Arenz, M.; Stamenkovic, V.; Wandelt, K.; Ross, P. N.; Markovic, N. M. *Surf. Sci.* **2002**, *506*, 287-296.

(67) Lin, W.-F.; Sun, S. G. *Electrochim. Acta* **1996**, *41*, 803-809.

(68) Zou, S.; Gomer, R.; Weaver, M. J. *J. Electroanal. Chem.* **2002**, *474*, 155-166.



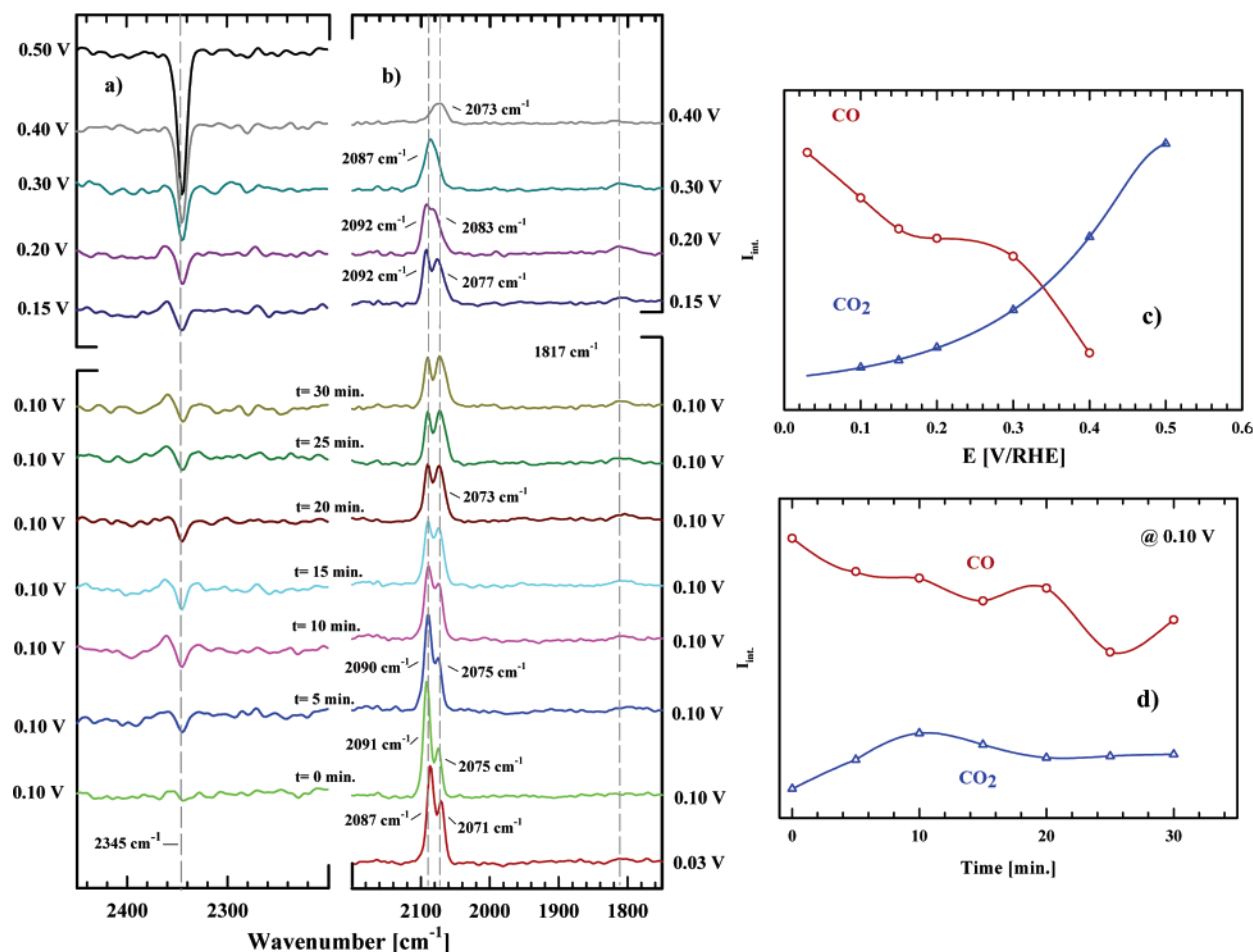
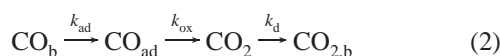


**Figure 6.** Time-resolved FTIR spectra for (a)  $\text{CO}_2$  production and (b) CO band morphology at different potentials. (c) Integrated intensities for  $\text{CO}_2$  production and  $\text{CO}_{\text{ad}}$  as a function of electrode potential in CO-saturated 0.5 M  $\text{H}_2\text{SO}_4$  solution. (d) Integrated intensities for  $\text{CO}_2$  production and  $\text{CO}_{\text{ad}}$  as a function of time in CO-saturated 0.5 M  $\text{H}_2\text{SO}_4$  solution.

solution are summarized in Figure 6c. Clearly,  $I_{\text{CO}_2}-E$  and  $I_{\text{CO}}-E$  plots show that the decrease in the CO intensity is mirrored by an increase in  $\text{CO}_2$  production, consistent with the L–H mechanism (eq 1) proposed above. Notice that although the oxidative removal of CO starts at very low potentials (ca 0.1 V in Figure 4), the slopes of the  $I_{\text{CO}_2}-E$  and  $I_{\text{CO}}-E$  plots are rather small, at least compared to the corresponding plots for CO oxidation on Pt(111) in acid solutions.<sup>49</sup> Although comparison of the IR intensities for chemisorbed CO on bimetallic surfaces and pure metals cannot be used in quantitative purposes,<sup>69</sup> difference in the  $I_{\text{CO}}-E$  plots between  $\text{Pt}_3\text{Sn}(111)$  and Pt(111) may suggest that the turn-over frequency for CO oxidation on  $\text{Pt}_3\text{Sn}(111)$  is lower relative to Pt(111) at potentials where there is nucleation of the  $\text{OH}_{\text{ad}}$  on both surfaces. The lower turnover rate on the former surface is possibly due to stronger adsorption and lower reactivity of the  $\text{OH}_{\text{ad}}$  on the Sn site versus Pt. Nevertheless, in general, the rate of CO oxidation on  $\text{Pt}_3\text{Sn}(111)$  depends on the delicate balance between the rate of re-adsorption ( $k_{\text{ad}}$ ) of  $\text{CO}_{\text{b}}$  on Pt sites created each time that  $\text{CO}_{\text{ad}}$  is oxidized ( $k_{\text{ox}}$ ) in the L–H type reaction (eq 2),



In FTIR experiments, if one takes into account that  $\text{CO}_2$  may slowly diffuse out of the thin-layer cell ( $\text{CO}_{2,\text{b}}$ ), then  $k_{\text{d}}$  in

reaction scheme (2) represents the rate of this diffusion. To see this balance in action, time-dependent changes in integrated intensities of  $\text{CO}_{\text{ad}}$  and  $\text{CO}_2$  are monitored at constant potentials. Figure 6 shows clearly that while  $I_{\text{CO}}$  decreases with time ( $\tau$ )  $I_{\text{CO}_2}$  has a tendency to increase with time, consistent with the L–H mechanism and continuous oxidation of CO even at this low potential. As discussed in our recent papers,<sup>15</sup> it turns out that this small activity is an important property for CO-tolerant catalysts. Closer examination of Figure 6d, however, reveals some time-dependent deviations, e.g.,  $I_{\text{CO}_2}$  first increases with time, reaching the maximum after ca. 10 min, and then, after a small decrease in  $I_{\text{CO}_2}$ , the production of  $\text{CO}_2$  reaches the steady-state value for  $\tau > 20$  min. To explain this we return to reaction scheme (2), which describes the possible reaction steps in the thin layer cell. Considering that  $I_{\text{CO}_2}$  is controlled by the delicate balance between the time-dependent diffusion of  $\text{CO}_2$  out of the thin layer cell ( $k_{\text{d}}$ ) and the production of  $\text{CO}_2$ , the latter being controlled simultaneously by the relation between  $k_{\text{ad}}$  and  $k_{\text{ox}}$ , we suggest that after the first 10 min  $k_{\text{ad}} + k_{\text{ox}} > k_{\text{d}}$ , for  $10 < \tau < 20$  min  $k_{\text{d}} > k_{\text{ad}} + k_{\text{ox}}$  and, finally, after ca. 20 min  $\text{CO}_2$  production probed by IR beam remains constant ( $k_{\text{ad}} + k_{\text{ox}} = k_{\text{d}}$ ).

(69) Rodriguez, J. A.; Truong, C. M.; Goodman, D. W. *J. Chem. Phys.* **2002**, *96*, 7814–7825.

(70) Faguy, P. W.; Marinkovic, N. S.; Adzic, R. R. *J. Electroanal. Chem.* **1996**, *407*, 209–218.

Another result from the time-resolved FTIR spectroscopy is the time-dependent change in the morphology of CO stretching bands and the appearance of the bridge-bonded CO even at 0.1 V. Figure 6 shows that initially ( $E = 0.1$  V and  $\tau = 0$ ) the bridging CO bend is absent and that the high-frequency band of atop CO has much higher intensity than the low-frequency band of atop CO. As time increases ( $\tau = 5$  min) the former band becomes less intense and simultaneously with CO oxidation ( $\text{CO}_2$  production at 0.1 V in Figure 6) a broad bridging CO frequency band, centered at ca.  $1817\text{ cm}^{-1}$ , appears in the spectra. The fact that the appearance of the bridge-bonded CO coincides with the onset of oxidation of CO suggests that the site occupancy of CO on the  $\text{Pt}_3\text{Sn}(111)$  surface is driven by the surface coverage of CO rather than by the applied electrode potential (field). Interestingly, after 30 min, the band intensity for high-frequency CO and low-frequency CO becomes the same. This behavior indicates that the oxidative removal of CO at low potentials proceeds first on the surface sites where local (microscopic) CO coverage remains high and thus CO is weakly adsorbed on Pt. Linking the microscopic and macroscopic levels of characterization, the weakly adsorbed ( $\text{CO}_{\text{ad}}^{\text{w}}$ ) state may correspond microscopically to the formation of disordered but compressed CO patches with characteristic high-frequency a-top CO IR bands. Furthermore, a pair of bands (centered at ca.  $2092$  and  $2077\text{ cm}^{-1}$ ) are transformed either into a single relatively broad peak centered at ca.  $2077\text{ cm}^{-1}$  at higher potentials (Figure 4) or, under steady-state conditions at lower potentials, into two peaks with the same intensities (Figure 6). Further inspection of Figures 4 and 6 reveals that both transitions are accompanied with the appearance of a new C–O stretching band (centered at ca.  $1820\text{ cm}^{-1}$ ) that can be related to the presence of bridge-bonded CO. It is this relaxed CO adlayer with a substantial alternation in the binding site geometry which was previously characterized as the strongly adsorbed state of  $\text{CO}_{\text{ad}}$  on the  $\text{Pt}_3\text{Sn}(111)$  surface.<sup>20</sup>

#### 4. Conclusions

In situ studies by surface X-ray scattering (SXS) and Fourier transform infrared (FTIR) spectroscopy are used to create a link between the detailed structure/composition of a  $\text{Pt}_3\text{Sn}(111)$  surface in an electrochemical environment and the macroscopic kinetic rates of the reacting system. The  $\text{Pt}_3\text{Sn}(111)$  single-crystal electrode was prepared and characterized in UHV prior to transfer into electrochemical cells. In agreement with previous work, the clean-annealed surface produced half-order spots in the LEED pattern, forming the  $p(2 \times 2)$  structure which is consistent with the surface composition, determined by LEIS, of 25 at. % Sn.

SXS results showed that the  $p(2 \times 2)$  structure can be transferred from UHV into 0.5 M  $\text{H}_2\text{SO}_4$  using the procedures developed in this laboratory. This structure remains stable, with the surface composition expected for the bulk termination, upon repeated potential cycling from 0.05 to 0.8 V. Adsorption of sulfuric acid anions on the  $p(2 \times 2)$  phase, which was studied by FTIR, produced a characteristic ‘butterfly-like’ feature in the CV of  $\text{Pt}_3\text{Sn}(111)$ . Detailed analysis of the SXS results revealed that expansion of surface atoms at 0.05 V, induced by adsorption of hydrogen, is ca. +2% from the bulk lattice spacing. At 0.5 V, where there is no hydrogen adsorption, the Pt atoms occupy bulk lattice positions but Sn atoms expand significantly, ca. 8.5%, i.e., there is significant buckling of the topmost atomic layer. SXS results also showed that the  $p(2 \times 2)$  structure is stable in a solution containing CO. In contrast to the  $\text{Pt}(111)$ –CO system, however, no ordered structures of CO were observed on the  $\text{Pt}_3\text{Sn}(111)$  surface and Pt in the topmost layer expands relatively little (ca. 1.5%) from the bulk lattice spacing upon the adsorption of CO, i.e., significantly smaller than the 4% expansion observed upon the adsorption of CO on  $\text{Pt}(111)$ . The difference in relaxation of these two surfaces covered by CO probably arises from the difference in the metal–adsorbate bonding, the  $\text{Pt}(111)$ –CO interaction being stronger than the  $\text{Pt}_3\text{Sn}(111)$ –CO interaction. The binding site geometry of CO on  $\text{Pt}_3\text{Sn}(111)$  was determined by FTIR. In contrast to the near invariant band of a-top CO on  $\text{Pt}(111)$ , changes in band shape (splitting of the band) and frequency (increase in the frequency mode) are clearly visible on the  $\text{Pt}_3\text{Sn}(111)$  surface. To explain the line shape of CO bands we suggest that, in addition to alloying effecting other factors, such as intermolecular repulsion between coadsorbed species, Sn atoms exists in two different chemical forms in the  $\text{Pt}_3\text{Sn}(111)$  surface and the high-frequency  $\text{CO}_{\text{ad}}$  occupies Pt atoms which are adjacent to ‘‘OH<sub>ad</sub>’’-covered Sn atoms, the low-frequency CO may occupy Pt sites in the vicinity of ‘‘non-oxidized’’ Sn atoms. The weakly adsorbed and more reactive form of  $\text{CO}_{\text{ad}}$  is that adsorbed next to the ‘‘OH<sub>ad</sub>’’-covered Sn atoms. Because of the weak adsorption, these sites are occupied only at high surface coverage of  $\text{CO}_{\text{ad}}$ , giving rise to a positive reaction order in  $p_{\text{CO}}$  for continuous oxidation of  $\text{CO}_b$  in solution.

**Acknowledgment.** This work was supported by the Director, Office of Science, Office of Basic Energy Sciences, Division of Materials Sciences, U.S. Department of Energy under Contract No. DE-AC03-76SF00098.

JA028771L